Inorganic Chemistry

Article

pubs.acs.org/IC

Organic–Inorganic Hybrid Materials Based on Basket-like $\{Ca\subset P_6Mo_{18}O_{73}\}$ Cages

He Zhang,[†,‡] Kai Yu,*[,†,‡] Jing-hua Lv,[†] Li-hong Gong,[†,‡] Chun-mei Wang,[†,‡] Chun-xiao Wang,[†,‡] Di Sun,[§] and Bai-Bin Zhou*[,†,‡]

[†]Key Laboratory for Photonic and Electronic Bandgap Materials, Ministry of Education, Harbin Normal University, Harbin 150025, P. R. China

[‡]Key Laboratory of Synthesis of Functional Materials and Green Catalysis, College of Heilongjiang Province, School of Chemistry and Chemical Engineering, Harbin Normal University, Harbin 150025, P. R. China

[§]School of Chemistry and Chemical Engineering, Shandong University, Jinan 250100, China

Supporting Information

ABSTRACT: Four basket-like organic–inorganic hybrids, formulated as $[\{Cu^{II}(H_2O)_2\}\{Ca_4(H_2O)_4(HO_{0.5})_3(en)_2\}\{Ca\subset P_6Mo_4{}^{V}Mo_{14}{}^{VI}O_{73}\}]\cdot 7H_2O$ (**1**), $(H_4bth)[\{Fe^{II}(H_2O)\}\{Ca\subset P_6Mo_{18}{}^{VI}O_{73}\}]\cdot 4H_2O$ (**2**), $(H_2bih)_3[\{Cu^{II}(H_2O)_2\}\{Ca\subset P_6Mo_2{}^{V}Mo_{16}{}^{VI}O_{73}\}]\cdot 2H_2O$ (**3**), $(H_2bib)_3[\{Fe^{II}(H_2O)_2\}\{Ca\subset P_6Mo_2{}^{V}\ Mo_{16}{}^{VI}O_{73}\}]\cdot 4H_2O$ (**4**), (bth = 1,6-bis(triazole)hexane; bih = 1,6-bis(imidazol)hexane; bib = 1,4-bis(imidazole)butane) have been hydrothermally synthesized and fully characterized. Compounds **1**–**4** contain polyoxoanion $[Ca\subset P_6Mo_n{}^{V}Mo_{18-n}{}^{VI}O_{73}]^{(6+n)-}$ (n = 0, 2, or 4) (abbreviated as $\{P_6Mo_{18}O_{73}\}$) as a basic building block, which is composed of a "basket body" $\{P_2Mo_{14}\}$ unit and a "handle"-liked $\{P_4Mo_4\}$ fragment encasing an alkaline-earth metal Ca^{2+} cation in the cage. Compound **1** exhibits an infrequent 2D layer structure linked by the $Cu(H_2O)_2$ linker and an uncommon tetranuclear calcium complex, while compound **2** is 8-connected 2-D layers connected by binuclear $\{Fe_2(H_2O)_3\}$ segaments, which are observed for the first time as 2-D basket-like assemblies. Compounds **3** and **4** are similar 1D Z-typed chains bonded by $M(H_2O)_2$ units (M = Cu for **3** and Fe for **4**). The optical band gaps of **1**–**4** reveal their semiconductive natures. They exhibit universal highly efficient degradation ability for typical dyes such as methylene blue, methyl orange, and rhodamine B under UV light. The lifetime and catalysis mechanism of the catalysts have been investigated. The compounds also show good bifunctional electrocatalytic behavior for oxidation of amino acids and reduction of NO_2^-.

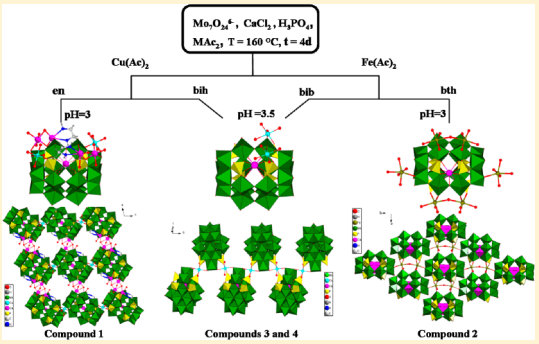

INTRODUCTION

The construction of polyoxometalate (POM)-based inorganic–organic hybrids, such as chains, layers, and nets, has been developed enormously in the past decades due to not only their diverse topological structures but also their potential applications in catalysis,[1] gas adsorption,[2] electromagnetism materials,[3] biomedicine,[4] and photochemistry.[5] The important feature of these hybrid assemblies is combination of the merit from inorganic and organic building blocks, which endows them with new structures and composite properties. POMs with definite sizes and shapes are unmatched inorganic components, which are inclined to bond with various linkage units, such as functional organic ligands,[6] rare earth metals,[7] transition metals,[8] and transition metal complex moieties.[9] The POMs characteristically maintain their identities in these modified POM derivatives. In addition, the synergic effects of components endow the derivatives with versatile properties in terms of redox chemistry, photochemistry, and charge distribution.[10] Thus, it is very important to choose appropriate POMs, metal linkage units, and organic ligands for functional inorganic–organic hybrid assemblies. Phosphomolybdate is undoubtedly one of the fastest growing branches in POM chemistry. In this subfamily, most hybrid compounds are based on Keggin-type $\{PMo_{12-x}TM_xO_{40}\}$, which is modified by various organic ligands and metal linkage units in different spatial packing modes.[11] In recent years, some new organic–inorganic hybrids based on $\{P_4Mo_6O_{31}\}$[12] and $\{P_2Mo_5O_{23}\}$[13] building blocks have been synthesized and characterized. However, compared with these phosphomolybdates, the basket-like $\{P_6Mo_{18}O_{73}\}$ kinds are undeveloped systems and are still less common. Basket-like POMs started relatively late and the first basket-type cluster, $[H_2dmpip]_5[K\subset P_6Mo_3{}^{V}Mo_{15}{}^{VI}O_{73}]$, was reported by Zhang in 2004.[14] Then basket-like hybrids modified by copper complexes, $[Cu(phen)(H_2O)_3][\{Cu(phen)(H_2O)_2\}\{Cu(phen)(H_2O)\}_3\{Sr\subset P_6\ Mo_4{}^{V}Mo_{14}{}^{VI}O_{73}\}]\cdot 3H_2O$[15] and $[Cu_4(bpy)_4(H_2O)_4K\subset P_6Mo_3{}^{V}Mo_{15}{}^{VI}O_{71}(OH)_2]\cdot 7H_2O$,[16] were

Received: March 4, 2015
Published: July 1, 2015

DOI: 10.1021/acs.inorgchem.5b00508
Inorg. Chem. 2015, 54, 6744–6757

reported. Recently, a series of basket hybrids modified by different transition metal complexes were reported by our group.[17] However, reduced basket-type polyoxoanions and their intermediates are usually unstable and hard to isolate from the solution. As a result, the numbers of basket-like POMs are still limited so far. Moreover, the coordination positions of the $\{P_6Mo_{18}\}$ heteropolyanion mainly occur at the oxygen atoms derived from four external phosphates and four molybdates in the handle of the "basket".[16] These active coordination sites are located on one side of the "basket". The facts lead to the larger steric limitations of basket-like POM, which is difficult to overcome in the modification process. Thus, most basket-type POMs are zero dimensional clusters, and only one example of a 1-D basket-like compound is reported so far.[18] The contexts provide us a large opportunity to extend basket clusters from 0D to 1D, 2D, and even 3D architectures. On the other hand, organic ligands play important roles in adjusting the construction of POM-based hybrid assemblies. They are important reducing agents to reduce Mo^{VI} into Mo^{V} centers in the formation of reduced POM-based hybrid.[19] They can lead to the condensation of the Mo^{VI} centered polyhedra in solution through the establishment of hydrogen-bonding interactions with the soluble intermediaries.[20] They can also induce the POM-based inorganic fragments to form different dimensions and various packing arrangements in the final hybrid materials via the formation of a variety of complex connection units or weak interaction modes.[21]

In our continuing research on the polymolybdate-based hybrids, basket-like assemblies were chosen as our research project based on the following reasons: (1) High dimensional basket-like hybrids can be obtained if flexible ligands or polynuclear complexes as the bridge unit are introduced into basket system. The larger steric hindrance of basket-like POMs can also be overcome if the molybdenum oxygen atoms of the "basket body" positions are activated in right reaction conditions. (2) Most basket-like POMs are obtained by using alkali metal K and alkaline earth metal Sr as template agents. Basket-like POMs encapsulating Ca^{2+} ions remain far less developed, and only two examples were reported so far. (3) Many basket-like POMs are partially reduced heteropoly blue, which can release a defined number blue electrons at appropriate redox ambiance. So they are potential reducing agents and exhibit interesting mixed-valence electron delocalization or electrochemical properties that are related to the electron-transfer reactions within the clusters. (4) The diffuse reflectivity spectrum shows that basket-like POMs having a band gap approximately in the range 2.7−3.2 can be regarded as wide gap semiconductor materials. Thus, basket-like POMs would be potential photocatalysts.

On the basis of the aforementioned considerations, we managed to overcome the larger steric hindrance of basket-like POMs and introduce Ca^{2+} into the basket-like POM system to act as template, which lead to four basket-like compounds from 1D chains to 2D layers, namely, $[\{Cu^{II}(H_2O)_2\}\{Ca_4(H_2O)_4(HO_{0.5})_3(en)_2\}\{Ca{\subset}P_6Mo_4{}^{V}Mo_{14}{}^{VI}O_{73}\}]\cdot 7H_2O$ (**1**), $(H_4bth)[\{Fe^{II}(H_2O)\}\{Ca{\subset}P_6Mo_{18}{}^{VI}O_{73}\}]\cdot 4H_2O$ (**2**), $(H_2bih)_3[\{Cu^{II}(H_2O)_2\}\{Ca{\subset}P_6Mo_2{}^{V}Mo_{18}{}^{VI}O_{73}\}]\cdot 2H_2O$ (**3**), $(H_2bib)_3[\{Fe^{II}(H_2O)_2\}\{Ca{\subset}P_6Mo_2{}^{V}Mo_{18}{}^{VI}O_{73}\}]\cdot 4H_2O$ (**4**). Electrochemical and photocatalytic properties of **1**−**4** have been investigated in detail.

EXPERIMENTAL SECTION

Materials and Measurements. All chemicals were commercially purchased and used without further purification. Elemental analyses (C, H, and N) were performed on a PerkinElmer 2400 CHN elemental analyzer; P, Mo, Fe, Cu, and Ca were analyzed on a PLASMA-SPEC (I) ICP atomic emission spectrometer. IR spectrum was recorded in the range 400−4000 cm^{-1} on an Alpha Centaurt FT/IR spectrophotometer using KBr pellets. X-ray photoelectron spectrum (XPS) analyses were performed on a VG ESCALAB MK II spectrometer with a Mg Kα (1253.6 eV) achromatic X-ray source. TG analyses were performed on a Perkin−Elmer TGA7 instrument in flowing O_2 with a heating rate of 10 °C·min^{-1}. XRD patterns were collected on a Rigaku Dmax 2000 X-ray diffractometer with graphite monochromatized Cu Kα radiation (λ = 0.154 nm) and 2θ ranging from 5° to 50°. UV−vis−NIR absorption spectroscopy was measured with a Cary 500 spectrophotometer. Diffuse reflectivity spectra were collected on a finely ground sample with a Cary 500 spectrophotometer equipped with a 110 mm diameter integrating sphere and were measured from 200 to 800 nm using barium sulfate ($BaSO_4$) as a standard with 100% reflectance. The electrochemical measurement was carried out on a CHI 660 electrochemical workstation at room temperature (25−30 °C).

Synthesis of $[\{Cu^{II}(H_2O)_2\}\{Ca_4(H_2O)_4(HO_{0.5})_3(en)_2\}\{Ca{\subset}P_6Mo_4{}^{V}Mo_{14}{}^{VI}O_{73}\}]\cdot 7H_2O$ (**1**). A mixture of $(NH_4)_6Mo_7O_{24}\cdot 2H_2O$ (2.048 g, 1.66 mmol), $Cu(Ac)_2\cdot H_2O$ (0.805g, 4.03 mmol), 1,2-ethylenediamine (0.289 g, 4.81 mmol), H_3PO_4 (1 mL, 15 mmol), $CaCl_2$ (0.782 g, 7.05 mmol), and H_2O (36 mL, 2 mol) was stirred at room temperature for 30 min; then the pH value was adjusted to about 3.0 with 1 M NaOH, and the mixture was sealed in a 50 mL Teflon-lined stainless steel reactor, which was heated at 160 °C for 4 days. The dark-blue crystals were isolated and collected by filtration, washed thoroughly with distilled water, and dried at room temperature (yield 47% based on Mo). Anal. Calcd for $C_4H_{41}Ca_5CuMo_{18}N_4O_{87.5}P_6$ (M_r = 3722.10): C, 1.29; H, 1.11; N, 1.51; P, 4.99; Cu, 1.71; Mo, 46.40; Ca, 5.38. Found: C, 1.27; H, 1.13; N, 1.49; P, 4.98; Cu, 1.73; Mo, 46.38; Ca, 5.41. IR (KBr pellet, cm^{-1}): 3439 (br), 3122 (sh), 1601 (s), 1492 (s), 1048 (s), 946 (s), 869 (s), 750 (s), 693 (s), 615 (s), 512 (s).

Synthesis of $(H_4bth)[\{Fe^{II}(H_2O)\}\{Ca{\subset}P_6Mo_{18}{}^{VI}O_{73}\}]\cdot 4H_2O$ (**2**). A mixture of $(NH_4)_6Mo_7O_{24}\cdot 2H_2O$ (2.048 g, 1.66 mmol), $Fe(Ac)_2\cdot 4H_2O$ (0.807 g, 3.28 mmol), 1,6-bis(triazole)hexane (0.312 g, 1.43 mmol), H_3PO_4(1 mL, 15 mmol), $CaCl_2$ (0.782 g, 7.05 mmol) and H_2O (36 mL, 2 mol) was stirred at room temperature for 30 min; then the pH value was adjusted to about 3.0 with 1 M NaOH, and the mixture was sealed in a 50 mL Teflon-lined stainless steel reactor, which was heated at 160 °C for 4 days. The dark-blue crystals were isolated and collected by filtration, washed thoroughly with distilled water, and dried at room temperature (yield 40% based on Mo). Anal. Calcd for $C_{10}H_{30}CaFeMo_{18}N_6O_{78}P_6$ (M_r = 3491.07): C, 3.44; H, 0.87; N, 2.41; P, 5.32; Fe, 1.60; Mo, 49.47; Ca, 1.15. Found: C, 3.42; H, 0.89; N, 2.43; P, 5.31; Fe, 1.59; Mo, 49.49; Ca, 1.13. IR (KBr pellet, cm^{-1}): 3398 (br), 1502 (s), 1415 (s), 1250 (m), 1041 (s), 967 (s), 843 (s), 756 (s), 698 (s), 636 (s), 548 (s).

Synthesis of $(H_2bih)_3\{Cu^{II}(H_2O)_2\}\{Ca{\subset}P_6Mo_2{}^{V}Mo_{18}{}^{VI}O_{73}\}]\cdot 2H_2O$ (**3**). A mixture of $(NH_4)_6Mo_7O_{24}\cdot 2H_2O$ (2.048 g, 1.66 mmol), $Cu(CH_3COOH)_2\cdot H_2O$ (0.814g, 4.08 mmol), 1,6-bis(imidazole)hexane (0.303 g, 1.39 mmol), H_3PO_4 (1 mL, 15 mmol), $CaCl_2$ (0.782 g, 7.05 mmol), and H_2O (36 mL, 2 mol) was stirred at room temperature for 30 min; then the pH value was adjusted to about 3.5 with 1 M NaOH, and the mixture was sealed in a 50 mL Teflon-lined stainless steel reactor, which was heated at 160 °C for 4 days. The dark-blue crystals were isolated and collected by filtration, washed thoroughly with distilled water, and dried at room temperature (yield 53% based on Mo). Anal. Calcd for $C_{36}H_{68}CaCuMo_{18}N_{12}O_{77}P_6$ (M_r = 3917.39): C, 11.04; H, 1.75; N, 4.29; P, 4.74; Cu, 1.62; Mo, 44.08; Ca, 1.02. Found: C, 11.06; H, 1.74; N, 4.28; P, 4.75; Cu, 1.64; Mo, 44.06; Ca, 1.01. IR (KBr pellet, cm^{-1}): 3437 (br), 3025 (m), 1536 (s), 1291 (s), 1061 (s), 968 (s), 875 (s), 807 (s), 745 (s), 671 (s), 521 (s).

DOI: 10.1021/acs.inorgchem.5b00508
Inorg. Chem. 2015, 54, 6744−6757

Table 1. Crystal Data and Structure Refinement Parameters for Compounds 1, 2, 3, and 4

compound	1	2	3	4
formula	$C_4H_{41}Ca_5Cu\ Mo_{18}N_4O_{87.5}P_6$	$C_{10}H_{30}CaFe\ Mo_{18}N_6O_{78}P_6$	$C_{36}H_{68}CaCu\ Mo_{18}N_{12}O_{77}P_6$	$C_{30}H_{60}CaFe\ Mo_{18}N_{12}O_{79}P_6$
M_r	3722.10	3491.07	3917.39	3861.57
cryst. size, mm^3	0.28 × 0.24× 0.22	0.22 × 0.20× 0.18	0.22 × 0.20× 0.18	0.22 × 0.20 × 0.18
cryst. syst.	monoclinic	orthorhombic	monoclinic	monoclinic
space group	*C*2/*c*	*Pnma*	*P*21	*P*2(1)/*c*
a, Å	14.0771(12)	32.334(3)	16.669(8)	22.503(5)
b, Å	27.041(2)	21.7718(17)	14.021(7)	13.701(3)
c, Å	24.569(2)	12.1888(10)	21.701(10)	30.208(6)
β, deg	102.344	90	104.734(8)	97.611(4)
V ($Å^3$)	9136.2(13)	8580.5(12)	4905(4)	9232(4)
Z	4	4	2	4
D_{calcd}, kg m^{-3}	2.706	2.703	2.652	2.778
μ(Mo Kα), mm^{-1}	3.112	2.985	2.696	2.791
F(000), e	7072.0	6592.0	3758.0	7392.0
θ range, deg	1.50−27.32	1.26−27.54	2.00−27.23	0.91−26.47
reflns collected/unique/Rint	25794/10199/0.0799	47690/9987/0.0824	28082/21623/0.0348	49761/18712/0.1192
data/restraints/params	10199/49/564	9987/18/562	19232/63/1361	18712/38/1324
R_1/wR_2 $[I \geq 2\sigma(I)]^a$	0.0855/0.1037	0.0633/0.0920	0.0405/0.0750	0.0626/0.0970
GoF $(F^2)^a$	1.073	1.091	1.026	1.035
$\Delta\rho_{fin}$ (max/min), e $Å^{-3}$	2.163/−2.152	2.383/−2.454	1.417/−0.838	2.277/−2.316

$^a R_1 = \sum||F_o| - |F_c||/\sum|F_o|$. $wR_2 = \{Rw[(F_o)^2 - (F_c)^2]^2/(Rw[(F_o)^2]^2)\}^{1/2}$.

*Synthesis of $(H_2bib)_3[\{Fe^{II}(H_2O)_2\}\{Ca\subset P_6Mo_2{}^{V}Mo_{18}{}^{VI}O_{73}\}]\cdot 4H_2O$ (**4**).* A mixture of $(NH_4)_6Mo_7O_{24}\cdot 2H_2O$ (2.048 g, 1.66 mmol), $Fe(Ac)_2\cdot 4H_2O$ (0.807 g, 3.28 mmol), 1,4-bis(imidazole)butane (0.302 g, 1.59 mmol), H_3PO_4(1 mL, 15 mmol), $CaCl_2$ (0.782 g, 7.05 mmol), and H_2O (36 mL, 2 mol) was stirred at room temperature for 30 min; then the pH value was adjusted to about 3.5 with 1 M NaOH, and the mixture was sealed in a 50 mL Teflon-lined stainless steel reactor, which was heated at 160 °C for 4 days. The dark-blue crystals were isolated and collected by filtration, washed thoroughly with distilled water, and dried at room temperature (yield 49% based on Mo). Anal. Calcd for $C_{30}H_{60}CaFeMo_{18}N_{12}O_{79}P_6$ (M_r = 3861.57): C, 9.33; H, 1.57; N, 4.36; P, 4.82; Fe, 1.45; Mo, 44.79; Ca, 1.04. Found: C, 9.37; H, 1.40; N, 4.35; P, 4.84; Fe, 1.43; Mo, 44.77; Ca 1.06. IR (KBr pellet, cm-1): 3428(br), 3067 (br), 1551 (s), 1443 (s), 1201 (m), 1043 (s),962 (s), 868 (s), 759 (s), 653 (s), 513 (s).

X-ray Crystallography. Single-crystal X-ray data of compounds **1**−**4** were collected on a Bruker SMART CCD diffractometer equipped with graphite monochromatized Mo Kα radiation (λ = 0.71073 Å). Semiempirical absorption corrections were applied using the SADABS program. The structure was solved by direct method and refined by the full-matrix least-squares methods on F^2 using the SHELXTL-97 software package.[22] All of the non-hydrogen atoms were refined anisotropically. Hydrogen atoms on carbon atoms of organic ligands were included at calculated positions and refined with a riding model. The H atoms on water molecules were not included and were just put into the final molecular formula. A summary of crystal data and structure refinement for compounds **1**−**4** is provided in Table 1. Selected bond lengths and angles for compounds **1**−**4** are listed in Tables S1−S4, Supporting Information. Crystallographic data for the structures have been deposited in the Cambridge Crystallographic Data Centre with CCDC 1051967 for **1**, 1051968 for **2**, 1051969 for **3**, and 1051966 for **4**.

Photodegradation Property Measurements. Photocatalytic properties of the samples were examined in conventional processes. Typically, compounds **1**−**4** (50 mg) were placed with 200 mL of dye (10 mg·L^{-1}) solution in a tubular quartz reactor and stirred in the dark for about 30 min to ensure adsorption equilibrium before irradiation. Then, the solution was stirred while being irradiated by the surrounding UV lamp of 125 W. At certain intervals, 5 mL of samples were taken out of the reactor and separated by centrifugation to remove suspended particles. Photodegradation of the separated sample was investigated by measuring the absorption spectra of the solution using a UV−vis spectrophotometer.

RESULTS AND DISCUSSION

Syntheses. Although the alkaline earth metal ions as template agents to stabilize and induce basket POMs have obtained great achievement,[17] to overcome the large steric hinderance and extend the dimensions for basket-like POMs has been still a challenging subject. Two strategies have been exploited to obtain basket-like hybrids with higher dimensions: (1) introduce flexible or longer linkers into the basket framework, such as a flexible ligand or polynuclear complexes; (2) activate the molybdenum oxygen atoms of the "basket body" positions and make them participate in coordination. In our initial reaction, different transition metals and rigid ligands are used in the system of Na_2MoO_4 as raw materials to result in a series of transition metal complex modified 0-D basket-like POMs. In order to overcome the steric hindrance, we tried to introduce a flexible nitrogen-containing ligand into the system. However, 0-D hybrids based on basket clusters and isolated ligands were obtained or no crystals could be obtained in these cases. It seems that Na_2MoO_4 does not match up with the flexible ligands. Thus, $(NH_4)_6Mo_7O_{24}$ was employed to substitute for Na_2MoO_4 in our reaction system. Fortunately, four basket-like hybrids from 1D chain to 2D layers were obtained under similar reaction conditions. One pot reactions of $(NH_4)_6Mo_7O_{24}\cdot 2H_2O$, H_3PO_4, $CaCl_2\cdot 6H_2O$, H_2O, and $TMAc_2$ were investigated by varying ligands and pH values of the reaction system. At the beginning, when bih and bib were added with the pH value at 3.5, two similar 1-D chains (compounds **3** and **4**, respectively) linked by $Cu(H_2O)_2$ and $Fe(H_2O)_2$ were obtained. When bib was replaced by bth at a lower pH value of 3.0 for **4**, 8-connected 2-D layers (compound **2**) based on $\{P_6Mo_{18}O_{73}\}$ polyanion and $Fe_2(H_2O)_3$ linker were prepared. When a flexible short ligand without an aromatic ring (en) was added into system **3**, with the pH value also decreased to 3.0, a basket-like 2-D layer supported by a $\{Cu(H_2O)_2\}$ linker and tetranuclear calcium complexes

DOI: 10.1021/acs.inorgchem.5b00508
Inorg. Chem. 2015, 54, 6744−6757

Scheme 1. Summary of the Extention of Basket-like POM from 1-D Chain to 2-D Layer via Varying Ligands and pH Values of the Reaction System

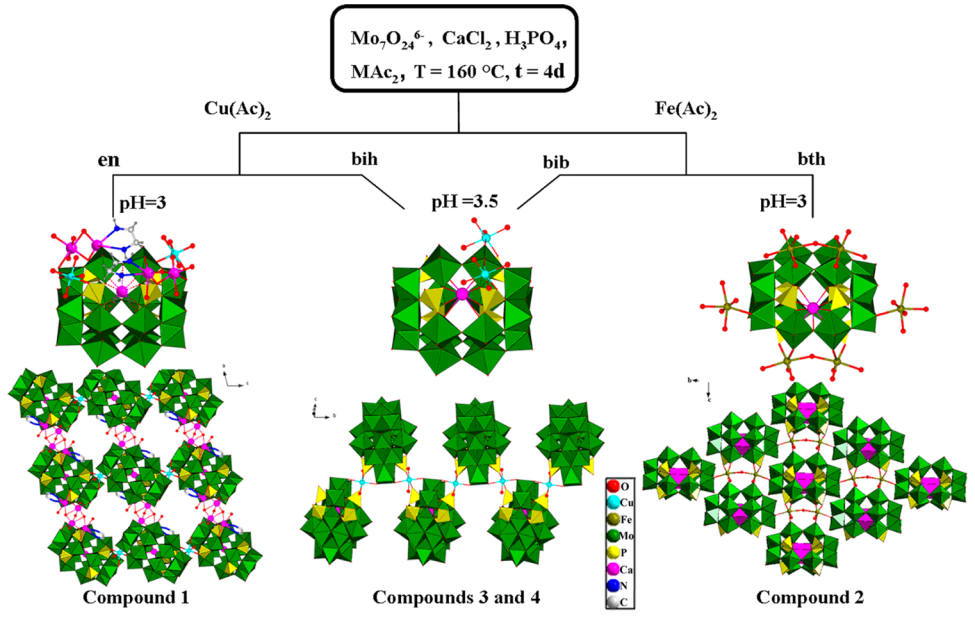

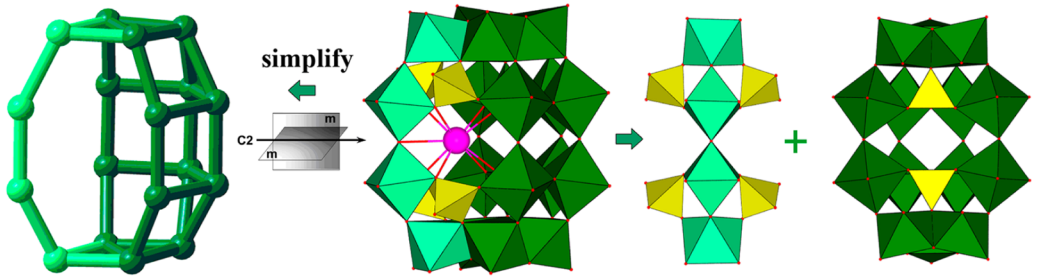

Figure 1. Polyhedral and ball-and-stick representation of basket-like $[CaC{\subset}P_6Mo_{18}O_{73}]^{n-}$ polyoxoanion consisting of the "handle" $\{P_4Mo_4\}$ unit and the "basket body" $\{P_2Mo_{14}\}$ unit.

$\{Ca_4(H_2O)_4((H_2O)_{0.5})_3\ (en)_2\}$ was formed. It is presumed that pH value and the type of ligand seem to be vital elements influencing the dimensions and packing arrangements of the compounds. The lower pH value (3.0) and a flexible long ligand with more N (bth) favor activation of oxygen atoms on the "basket body" positions, resulting in a highly connected 2D layer structure. While the same pH (3.0) and a flexible short ligand (en) tends to form polynuclear complexes, which also lead to 2-D layers. The results indicate that introduction of polynuclear complexes and activation the oxygen atoms of the "basket body" positions are two valid ways to extend the dimensions of basket-like POM. In fact, the longer flexible ligands (bth, bih, and bib in compounds **2**−**4**) tend to be protonated at lower pH values of basket system and fail to bond to TM ions. However, these organic ligands are essential during the synthesis, and in a series of similar reactions without the ligands, no crystals could be obtained. The ligands are important reducing agents to reduce Mo^{VI} into Mo^{V} centers in the formation of mixed valence basket-like POM. On the other hand, they can induce the $\{P_6Mo_{18}O_{73}\}$-based segments to form different dimensions or various packing arrangements in the final hybrid materials. It is unsuccessful for our attempts to use only Cu or Fe to induce compounds **1**−**4**, which shows that the kind of TM also affects the formation of these compound. The formations of these complexes are shown in Scheme 1. Although scarce 1-D and 2-D basket-like POMs are obtained via adjusting pH and the kind of organic ligand in our hydrothermal syntheses, the isolation of 3D highly connected covalent hybrids based on the basket POM still remains a great challenge to us.

Structure Descriptions. Compounds **1**−**4** consist of similar basket-like $[CaC{\subset}P_6Mo_n{}^{V}Mo_{18-n}{}^{VI}O_{73}]^{(6+n)-}$ (n = 0, 2, or 4) polyoxoanions, which comprise two sections: a tetralacunary γ-Dawson $\{P_2Mo_{14}\}$ fragment and a handle-like $\{P_4Mo_4\}$ unit (Figure 1). The $\{P_2Mo_{14}\}$ cluster stems from the γ-Dawson polyoxoanion by removal of four adjacent $\{MoO_6\}$ octahedra of equatorial position to form the "basket body". The $\{P_4Mo_4\}$ segment is composed of four $\{MoO_6\}$ octahedra and four $\{PO_4\}$ tetrahedra, which are linked in a corner-sharing mode to form the "handle" of the basket. The two sections are connected in edge- and corner-sharing ways to form the basket-like cage with C_{2v} symmetry (see Figure 1). All Mo centers display a octahedron coordination geometry with Mo−O bond lengths in the range of 1.659(6)−2.456(10) Å and O−Mo−O bond angles varying from 84.5(4)° to 174.8(6)°. The six P centers exhibit tetra-coordination. The P−O bond lengths range from 1.46(2) to 1.600(5) Å, while the O−P−O bond angles vary from 105.5(3)° to 114.2(11)° (Tables S1−S4, Supporting Information). In the central space of the polyoxoanion, a Ca^{2+} ion is encapsulated, showing eight/

DOI: 10.1021/acs.inorgchem.5b00508
Inorg. Chem. 2015, 54, 6744−6757

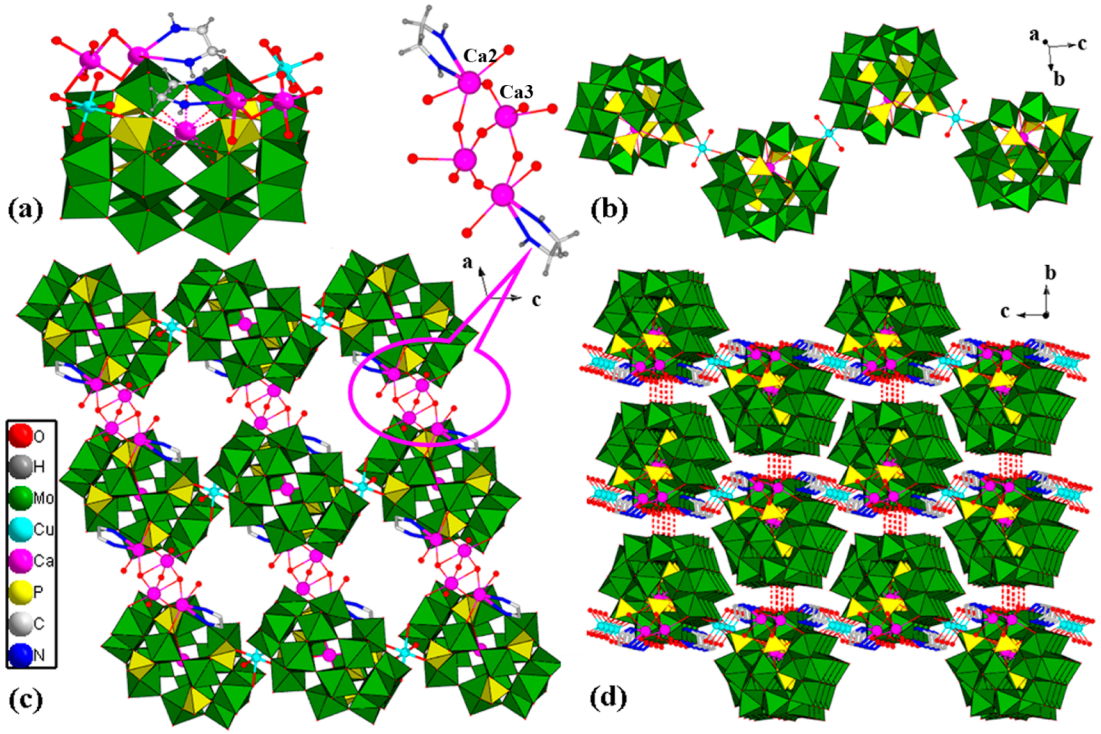

Figure 2. (a) Coordination pattern of $\{P_6Mo_{18}O_{73}\}$ cluster of compound **1**, (b) 1-D chain of compound **1** based on $\{P_6Mo_{18}\}$ units and $\{Cu(H_2O)_2\}$ linkers, (c) 2-D supramolecular layer of compound **1** linked by tetracalcium complexes $\{Ca_4(H_2O)_4(HO_{0.5})_3(en)_2\}$ and (d) 3-D supramolecular network on the *bc* plane of compound **1**.

nine-coordination with bond lengths of Ca−O in the range of 2.453(9)−2.842(12) Å. It is proved that the space size of the basket-like cluster tended to capture larger alkali metals or alkaline earth cations.[15,17] In fact, the incorporation of the large cations can also stabilize the basket-like cage.

Crystal Structure of 1. Compound **1** crystallizes in the space group *C*2/*c* and exhibits 2D layer structure linked by the $Cu(H_2O)_2$ linker and an uncommon tetranuclear calcium complex. The asymmetric unit of compound **1** contains a four-electron reduced $\{CaCP_6Mo_4{}^{V}Mo_{14}{}^{VI}O_{73}\}^{10-}$ polyoxoanion, one $\{Cu(H_2O)_2\}^{2+}$ linker, one tetranuclear calcium complex $\{Ca_4(H_2O)_4(HO_{0.5})_3\ (en)_2\}$ unit, and seven water molecules (Figure S1, Supporting Information). There is one kind of crystallographically independed Cu atom, which exhibits octahedral coordination geometry with four terminal oxygen atoms from two adjacent basket clusters and two water molecules (Figure 2a,b). The Cu−O distances are in the range of 1.92(2)−2.54(8) Å. The O−Cu−O angles are in the range of 88.9(8)−179.99(6) Å. In addition, There are three crystallographically independent Ca atoms, which exhibit three kinds of coordination geometries coexisting in structure **1**. Ca1 in the central cavity of the basket cage shows nine-coordination with the bond lengths of Ca1−O in the range of 2.535(18)−2.83(3) Å. Ca2 atom shows a six-coordinated environment, which is defined by two nitrogen atoms from one en organic ligand, two terminal oxygen atoms from one basket cluster, one water molecular, and one μ-O shared by two Ca atoms. Each Ca3 atom completed its octahedral coordination geometry with two terminal oxygen atoms from one basket cluster, one water molecular, and three μ-O atoms. It is worth mentioning that O40 and O39 are half-occupied. The average bond lengths of Ca−O and Ca−N are 2.31 and 2.56 Å, respectively. In this linkage mode, four Ca centers and two en ligands are bonded together by five μ-O bridges to form unusual tetranuclear complexes $\{Ca_4(H_2O)_4(HO_{0.5})_3(en)_2\}$ (Figure 2c). Each basket-like anion connected with two adjacent basket-type clusters through two $\{Cu(1)(H_2O)_2\}$ fragments to generate infinite 1-D wave-liked chains (Figure 2b). The adjacent chains are further bonded together by tetranuclear segments $\{Ca_4(H_2O)_4(HO_{0.5})_3(en)_2\}$ to form the 2-D layer (Figure 2c). In the structure, four basket-like clusters are alternately bridged by two $\{Cu(1)(H_2O)_2\}$ linkers and two tetranuclear complexes to form big apertures with dimensions of 9.47 Å × 14.07 Å (O(42)−C(42) 9.47 Å and Cu(1)−Cu(1) distance 14.07 Å). Moreover, the 3D supramolecular framework (Figure 3d) was generated by supramolecular interactions between surface oxygens of adjacent 2D layers with O10··· O24

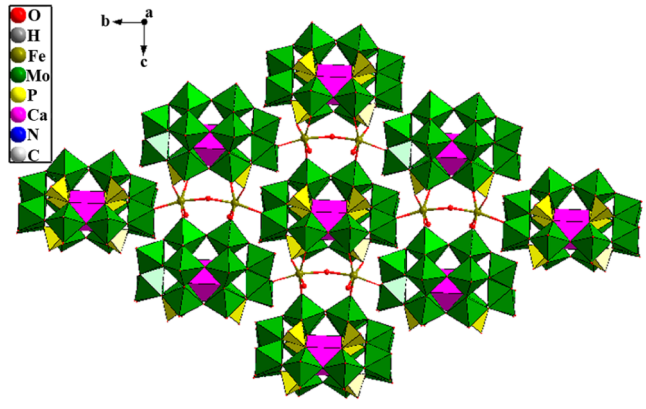

Figure 3. Two-dimensional layer of compound **2** based on $\{P_6Mo_{18}O_{73}\}$ units and $\{Fe_2(H_2O)_3\}$ linkers.

DOI: 10.1021/acs.inorgchem.5b00508
Inorg. Chem. 2015, 54, 6744−6757

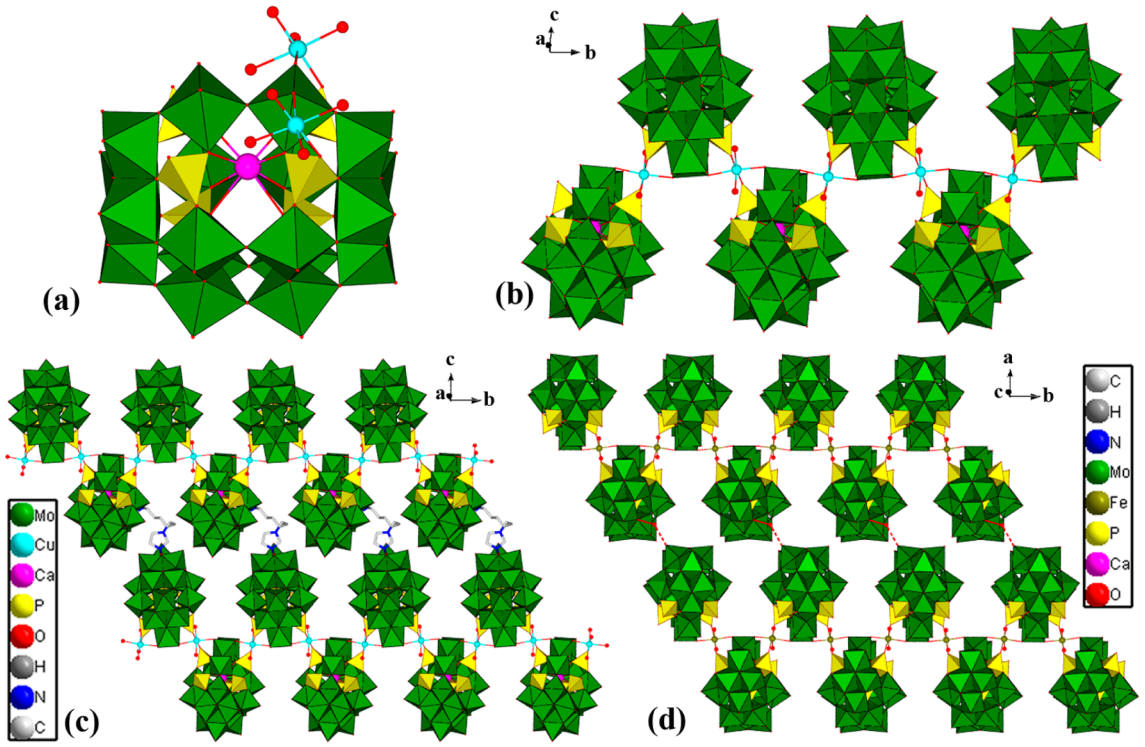

Figure 4. (a) Coordination pattern of the $\{P_6Mo_{18}O_{73}\}$ unit of compound **3**, (b) 1-D chain of compound **3** based on $\{P_6Mo_{18}O_{73}\}$ units and $\{Cu(H_2O)_2\}$ linkers, (c) 2-D supramolecular layer of compound **3** linked by protonated H_2bih ligand, and (d) 2-D supramolecular layer of compound **4** connected by water molecules.

= 2.920 Å (Figure 2d). All solvent water molecules reside in the interspaces between two adjacent layers.

Crystal Structure of **2**. Compound **2** is built up of a fully oxidized basket-like polyoxoanion $\{Ca\subset P_6Mo_{18}{}^{VI}O_{73}\}^{6-}$ cluster, one $\{Fe(H_2O)\}^{2+}$ ions, one protonated H_4bth ligand, and two water molecules (Figure S2, Supporting Information). In compound **2**, there is one kind of crystallographically independent Fe atom, which exhibits octahedral coordination geometry with four terminal oxygen atoms from three different basket clusters and two water moleculars. The Fe−O distances are in the range of 1.904(3)−2.534(4) Å. The O−Fe−O angles are in the range of 91.6(10)−168.1(11) Å. It is interesting that two adjacent Fe1 atoms are linked by a common water (O2W) to form binuclear $\{Fe_2(H_2O)_3\}$ fragments. Each binuclear $\{Fe_2(H_2O)_3\}$ segment connects four different basket-like polyoxoanions. Meanwhile each basket-like polyoxoanion as an octadentate ligand links four $\{Fe_2(H_2O)_3\}$ units through eight terminal oxygen atoms (Figure S3, Supporting Information). In this way, each basket-like polyoxoanion connected with eight adjacent basket-type clusters through four $\{Fe_2(H_2O)_3\}$ linkers to generate 8-connected 2-D layers (Figure 3). Moreover, these adjacent 2-D layers are further supported by a supramolecular interaction (O24···O24 2.911 Å) (Figure S4, Supporting Information) between terminal oxygen atoms of two adjacent 2D layers to yield extending 3-D network structure.

Crystal Structures of **3** *and* **4**. Compounds **3** and **4** are similar 1D chains with only slight differences in species of transition metals and protonated organic ligand, and the number of water molecules. The basic units consist of a two-electron reduced polyoxoanion $\{Ca\subset P_6Mo_2{}^{V}Mo_{16}{}^{VI}O_{73}\}$ cluster, one $\{M(H_2O)_2\}$ (M = Cu for **3** and Fe for **4**) linker, three protonated H_2bih or H_2bib ligands, and four or two lattice water molecules (Figures S5 and S7, Supporting Information). There is one crystallographically independent M^{2+} cation that forms an octahedral configuration with four terminal oxygen atoms from two adjacent basket-like clusters and two oxygen donors from coordinated water molecules. The bond distances of Cu−O and Fe−O are in the range of 1.948(6)−2.210(6) Å and 2.032(10)−2.222(9) Å, respectively. The angles of O−Cu−O and O−Fe−O are in the range of 83.5(2)−178.6(2)° and 87.6(4)−175.2(4)°, respectively. In this connection mode, each basket cluster connects with adjacent two basket units in ABAB mode via transition metal $\{M(H_2O)_2\}^{2+}$ fragments to form infinite 1D zigzag chains (Figure 4b and Figure S8, Supporting Information). The adjacent zigzag chains are parallel to each other and are further aggregated together to yield a 2D supramolecular layer via protonated H_2bih ligands with hydrogen bond interactions (N4···O14 2.951(10) Å and N3···O13 2.987(11) Å) (Figure 4c) or supramolecular interactions (O59···O1W 2.878 and O1W···O74 2.845 Å) between lattice water molecules and terminal oxygen atoms of two adjacent 1D chains (Figure 4d). The 3D supramolecular framework (Figures S6 and S9, Supporting Information) was generated by hydrogen bonds (N8···O14 2.930(11)) between protonated H_2bih ligands and terminal oxygen atoms of adjacent 2-D layers or weak interactions between water molecules and oxygen atoms of the polyoxoanion in different 2D layers (O3W···O75 2.926(16) Å and O3W···O31 2.633 Å). All bond lengths and bond angles of hydrogen bonds for compounds **1**-**4** are shown in Table S5, Supporting Information.

Bond-valence sum (BVS) calculations[23] show an average value of ca. 5.78 for Mo centers in compound **1**, which is close to the result of 14 Mo^{6+} and four Mo^{5+} in the polyoxoanion cluster. BVS results are approximately 5.96 for Mo centers in

DOI: 10.1021/acs.inorgchem.5b00508
Inorg. Chem. 2015, 54, 6744−6757

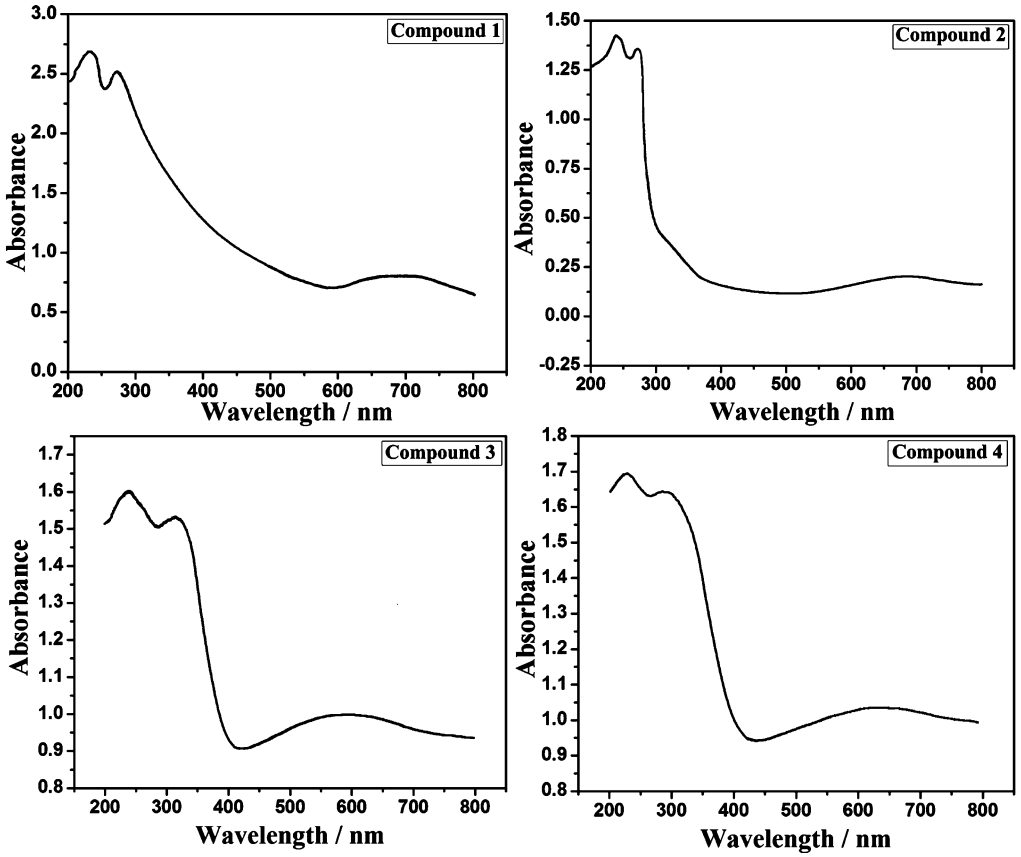

Figure 5. UV−vis spectra of compounds **1**−**4** in solid state at room temperature.

compound **2**, indicating that their oxidation states are +6. BVS calculations display an average value of ca. 5.86 and 5.87 for Mo centers in compounds **3** and **4**, respectively, which is about the result of 16 Mo^{6+} and two Mo^{5+} in the polyoxoanion (Tables S6−9, Supporting Information). In addition, BVS calculations confirm that all P centers are in the oxidation states of +5, and Ca centers in compound **1**−**4**, Cu centers in compounds **1** and **3**, and Fe centers in compounds **2** and **4** are in the oxidation states of +2. Moreover, four or two extra protons should be added to the organic agents in compounds **2** and **4**, respectively, for charge balance. Thus, compounds **1**−**4** can be formulated as above.

Spectroscopic and Thermal Analysis. *IR Spectra Analyses.* The IR spectra of compounds **1**−**4** recorded between 400 and 4000 cm^{-1} with KBr pellet (Figure S10a−d, Supporting Information) are similar: the peaks at 1250−1041 cm^{-1} are attributed to ν(P−Oa) vibrations; the strong peaks at 968−946 cm^{-1} are ascribed to $\nu(Mo{=}O_{terminal})$ vibrations; peaks at 875−745 cm^{-1} are assigned to $\nu(Mo{-}O_{bridge})$ vibrations. The peaks located at 512−698 cm^{-1} can be attributed to ν(TM−O).[24] The strong peaks at 1401−1492 cm^{-1} are indicative of ν(C−N) vibrations of organic ligands. Furthermore, the broad peaks between 3025 and 3439 cm^{-1} and the peaks at 1502−1601 cm^{-1} can be assigned to ν(N−H) or ν(O−H) of the protonated ligands and water molecules.

XPS Spectra Analyses. The oxidation states of Mo are further confirmed by X-ray photoelectron spectroscopy (XPS) measurements, which were carried out in the energy region of Mo $3d_{5/2}$ and Mo $3d_{3/2}$ (Figure S11a−d, Supporting Information). The XPS spectra of compounds **1**, **3**, and **4** present four overlapped peaks at 230.9−231.1, 234.1−234.3, 235.1−235.3, and 232.4−232.6 eV in the Mo 3d region, which should be ascribed to the mixture of Mo^{5+} and Mo^{6+}, respectively.[25] The XPS spectrum of **2** presents two peaks at 232.3 and 235.2 eV, in the Mo 3d region, which should be assigned to Mo^{6+}. The XPS results also support the BVS calculations for the Mo oxidation states, in which the deconvolution of the spectra indicates that the ratio of Mo^{VI}/Mo^{V} is about 7:2 for compound **1** and about 8:1 for compounds **3** and **4**, respectively.

XRPD Analysis. The simulated and experimental the X-ray power diffraction (XRPD) patterns of the compounds **1**−**4** are presented in Figure S12a−d, Supporting Information. The diffraction peaks of both simulated and experimental patterns match in the key positions, indicating the phase purity of the compounds. The difference in intensity may be due to the preferred orientation of the powder samples.

Thermogravimetric (TG) Analysis. The thermal stabilities of compounds **1**−**4** were investigated under an O_2 atmosphere from 40 to 800 °C, and the TG curves are shown in Figure S13a−d, Supporting Information. The TG curves show two major weight losses for compounds **1**−**4**. The first weight loss of 6.96% at 120−270 °C for **1**, 2.49% at 175−290 °C for **2**, 1.85% at 150−235 °C for **3**, and 2.72% at 170−240 °C for **4** corresponding to the loss of all lattice water and coordinated water molecules (calcd 7.02% for 14.5 H_2O, 2.58% for 5 H_2O, 1.84% for 4 H_2O, and 2.81% for 6 H_2O, respectively). The second weight losses at 410−620 °C of 2.93% for **1**, 390−630 °C of 6.51% for **2**, 360−580 °C of 16.64% for **3**, 400−570 °C of 14.92% for **4** arise from the losses of protonated ligands (calcd 3.23% for two en, 6.43% for one bth, 16.87% for three bih, and 14.96% for three bib, respectively). All the weight loss

DOI: 10.1021/acs.inorgchem.5b00508
Inorg. Chem. 2015, 54, 6744−6757

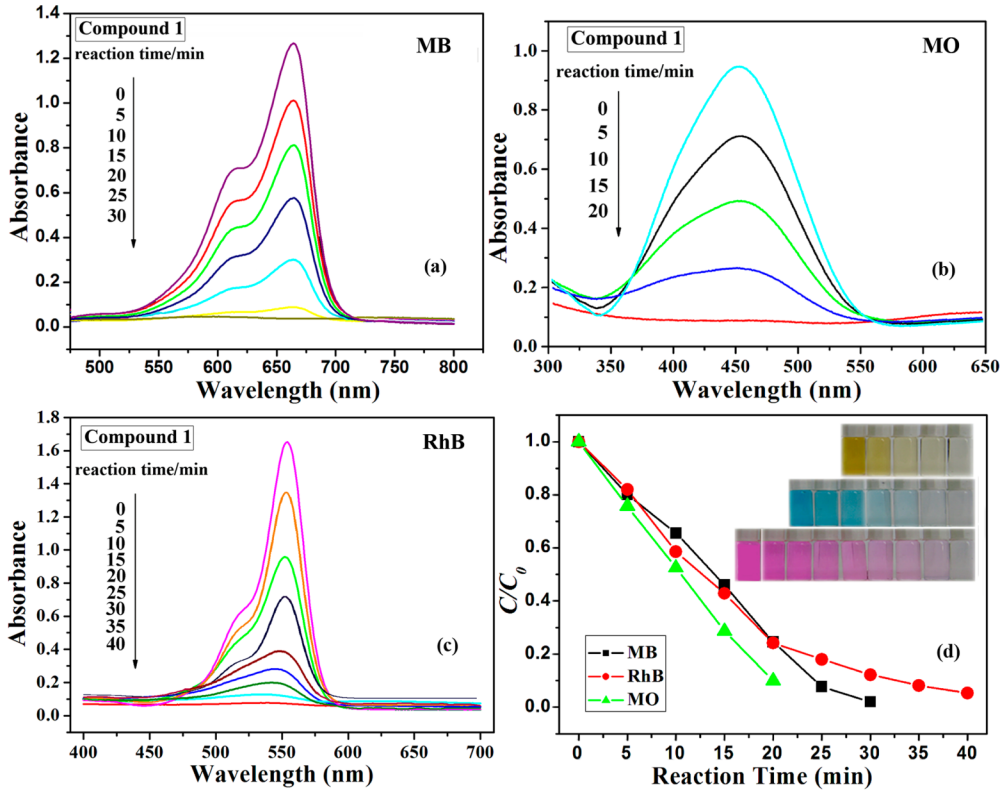

Figure 6. UV−vis absorption spectra of (a) MB, (b) MO, and (c) RhB solution during the decomposition reaction under UV irradiation in the presence of compound **1** and (d) plot of irradiation time versus concentration for MB, MO, and RhB in the presence of compound **1**.

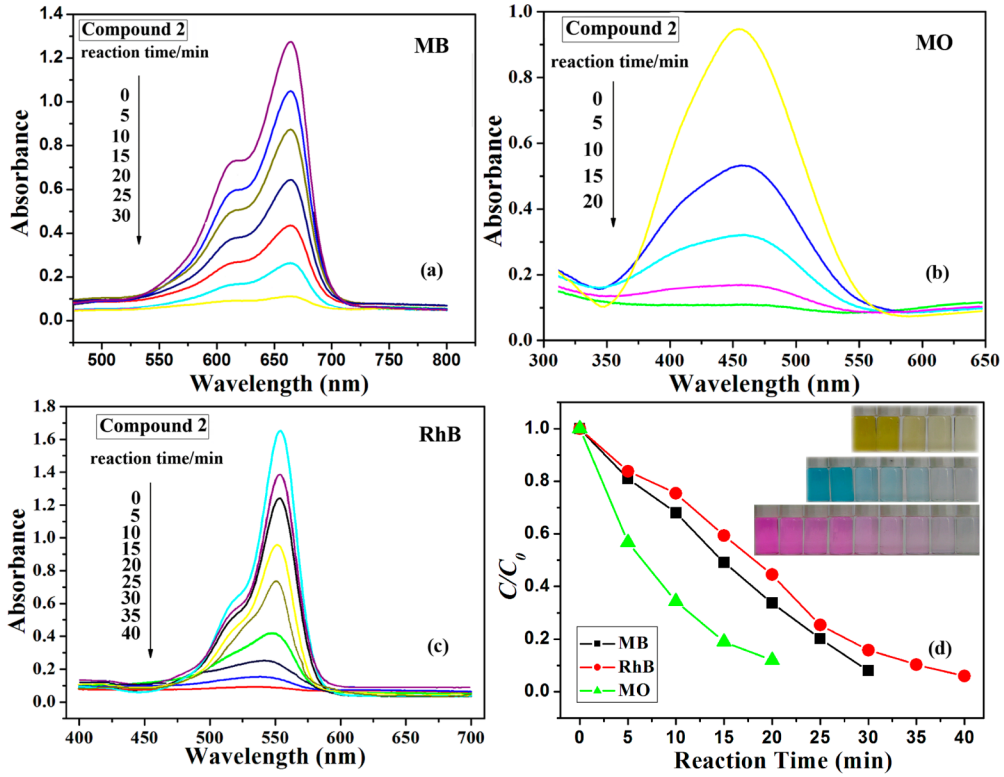

Figure 7. UV−vis absorption spectra of (a) MB, (b) MO, and (c) RhB solution during the decomposition reaction under UV irradiation in the presence of compound **2** and (d) plot of irradiation time versus concentration for MB, MO, and RhB in the presence of compound **2**.

from the TG curves accord with the formulas of compounds **1**−**4**.

UV Spectral Analyses and Optical Band Gap. The UV−vis absorption spectra of compounds **1**−**4** were conducted in solid

DOI: 10.1021/acs.inorgchem.5b00508
Inorg. Chem. 2015, 54, 6744−6757

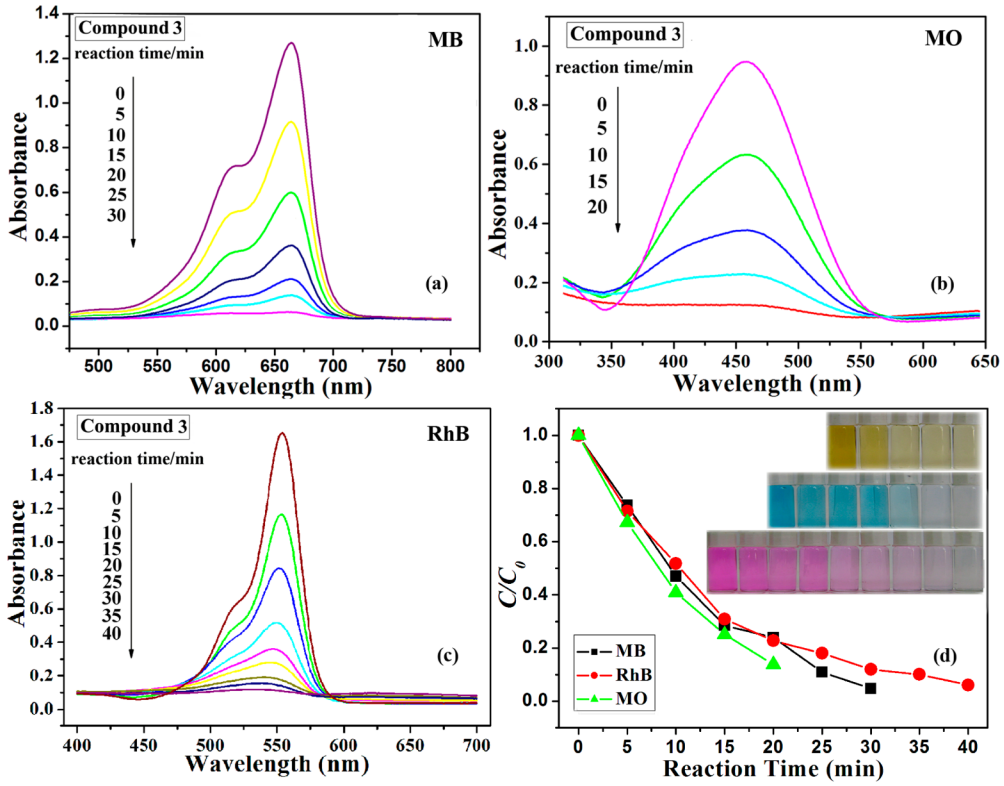

Figure 8. UV−vis absorption spectra of (a) MB, (b) MO, and (c) RhB solution during the decomposition reaction under UV irradiation in the presence of compound **3** and (d) plot of irradiation time versus concentration for MB, MO, and RhB in the presence of compound **3**.

state at room temperature (shown in Figure 5). The two strong bands in the range of 223−241 nm and 279−314 nm are attributed to $p\pi(O_{terminal}) \rightarrow d\pi^*(Mo)$ electronic transitions in the Mo═O bonds and $d\pi-p\pi-d\pi$ electronic transitions between the energetic levels of the Mo−O−Mo bonds, respectively.[24] The broad band at 580−675 nm ascribed to the intervalence transition from the Mo^{V} to Mo^{VI} via the Mo−O−Mo bond or the d−d transitions of Mo^{V} octahedra.[24]

The studies of diffuse reflectivity for powder samples of **1**−**4** were employed to gain their band gaps (E_g), which were determined as the intersection point between the energy axis and the line extrapolated from the linear portion of the adsorption edge in a plot of Kubelka−Munk function F versus energy E.[26] As shown in Figure S14a−d, Supporting Information, the E_g values assessed from the steep absorption edge of compounds **1**−**4** are 2.75 eV for **1**, 3.08 eV for **2**, 2.94 eV for **3**, and 2.97 eV for **4**. The reflectance spectra reveal the presence of an optical band gap and the semiconductive properties with a wide band gap for the compounds. Thus, compounds **1**−**4** would be potential photocatalysts.

Photocatalysis Properties of Compounds 1−4. The photocatalytic activities of compounds **1**−**3** were evaluated for degradation of methyl orange (MO), methylene blue (MB), and rhodamine B (RhB) under UV irradiation (compounds **3** and **4** are similar 1-D chains, so only photocatalytic activities of compound **3** are studied as an example). The absorption peaks of MO, MB, and RhB decreased obviously with increasing reaction time and nearly disappeared after degradation reaction. (Figures 6−8). The absorption bands were not shifted, and no new absorption peak occurred in the figures, which showed that benzene or heterocycles were destroyed during the reaction. The photocatalytic decomposition rates ($1 - C/C_0$) are 98.27% of MB, 90.38% of MO, and 95.32% of RHB for **1**, 90.14% of MB, 87.17% of MO, and 94.06% of RHB for **2**, 96.53% of MB, 87.62% of MO, and 94.28% of RHB for **3** after 30, 20, and 40 min, respectively. The colors of the three dye solutions also became weak gradually with the increase of time, finally almost disappearing. The facts above show that basket-type POMs are good photocatalysts, which have universal high efficiency to degrade typical dyes such as MB, MO, and RhB. Compared with reported Keggin and Dawson hybrid POMs, compounds **1**−**3** exhibit better degradation ability for typical dyes in shorter time under similar reaction conditions.[27] For example, only 63% and 94% of MB were decomposed by the Keggin- and Dawson-based hybrid after 180 min in ref 27a. In addition, the degradation efficiencies of **1** under UV light are higher than others, which may arise from two reasons. First, tetranuclear calcium complexes as bridging units promote the transfer of the electron from POM to POM, which facilitates electron transfer to the surface of POM. Second, the large pores in compound **1** increase the contact area between catalysts and substrate and promote more active centers to be involved in the catalytic reactions. The decomposition rates of compound **2** seem to be the lowest in the three compounds, which may be due to its larger space occupied. The larger steric effects in the highly connected basket layer tend to hinder the migration and mobility of excited holes and electrons to the surfaces.

The repeated use of the catalyst can reduce the cost of the photocatalytic processes. In order to evaluate the lifetime of catalysts, compounds **1**−**3** were recycled five times to degrade MB at same reaction conditions. As shown in Figure 9, the photocatalytic activity of compounds **1**−**3** was nearly maintained and decreased slightly when they were recycled four times. In the fifth cycle, the catalytic efficiency declined greatly for the losses in the amount of catalysts. Furthermore, The XRD spectra of compounds **1**−**3** before and after five

DOI: 10.1021/acs.inorgchem.5b00508
Inorg. Chem. 2015, 54, 6744−6757

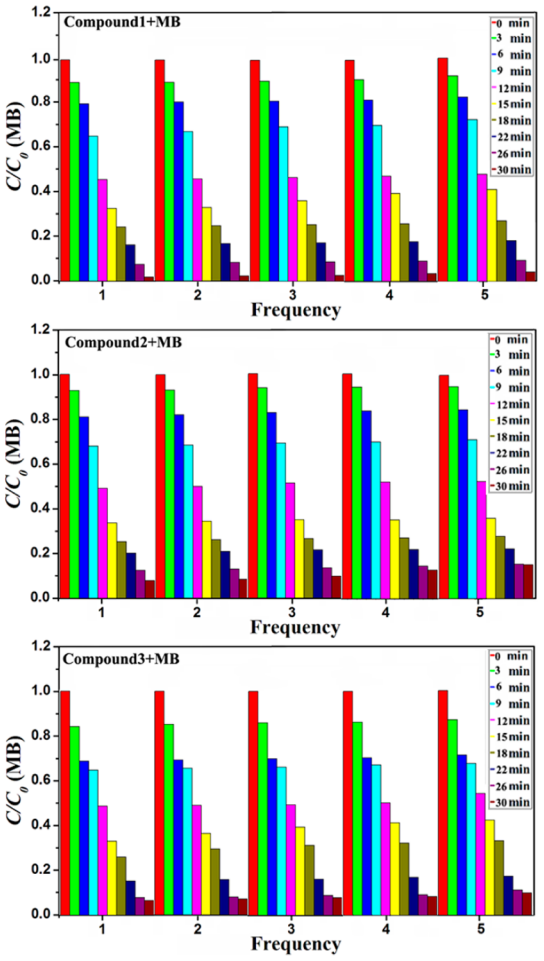

Figure 9. Effect of catalyst reuse on the degradation of MB after 30 min under UV light.

cycles of photocatalytic reaction are shown in Figure S15, Supporting Information. Comparing the XRD pattern of the three compounds before and after recycle reactions, both the position and the intensity of the peaks were nearly identical. The above results suggest that compounds **1**−**3** have excellent repeatability and stability, which has important implications for the practical application of photocatalyst.

To understand photocatalytic reaction mechanism of basket-type POMs in-depth, compound **1** was chosen as a representative to investigate degradation pathways of dyes. UV irradiation of compound **1** would induce charge transfer from the HOMO of nonbonding oxygen to the LUMO of molybdenum, and then photogenerated electron−hole pairs are formed.[28] The photogenerated electron and hole are separated by overcoming mutual electrostatic attraction to migrate to the surface of the basket-like POM, where the electron will be captured by O_2 to form $^{\bullet}O_2^-$. The $^{\bullet}O_2^-$ radicals can react with H^+ ions and electrons to produce $^{\bullet}OH$ radicals. The photogenerated hole can also transform into $^{\bullet}OH$ through reacting with H_2O or OH^- ions. The possible mechanism of photocatalytic reaction is as shown in eqs 1-6):

$$\{P_6Mo_{18}O_{73}\} + h\nu \rightarrow \{P_6Mo_{18}O_{73}\}(e^-) + h^+ \quad (1)$$

$$\{P_6Mo_{18}O_{73}\}(e^-) + O_2 \rightarrow \{P_6Mo_{18}O_{73}\} + {}^{\bullet}O_2^- \quad (2)$$

$${}^{\bullet}O_2^- + 2H^+ + e^- \rightarrow H_2O_2 \quad (3)$$

$$H_2O_2 + e^- \rightarrow {}^{\bullet}OH + OH^- \quad (4)$$

$$OH^- + h^+ \rightarrow {}^{\bullet}OH \quad (5)$$

$$H_2O + h^+ \rightarrow {}^{\bullet}OH + H^+ \quad (6)$$

In the photoreaction equations, superoxide radicals ($^{\bullet}O_2^-$), hydroxyl radicals ($^{\bullet}OH$), and photogenerated holes (h^+) are active species of oxidation dyes for degradation reaction. In order to confirm degradation pathways of dyes over basket-like POMs, a series of radical trapping experiments for compound **1** on different substrates were performed by using of benzoquinone (BQ) and dimethyl sulfoxide (DMSO) scavengers. The BQ and DMSO are effective scavengers for $^{\bullet}O_2^-$ and $^{\bullet}OH$ radicals, respectively. Compared with the reaction without adding radical scavengers, decomposition rates of MB only dropped 13.14% and 14.81%, respectively, with addition of BQ and DMSO (Figure 10a). This demonstrates that the photogenerated h^+ is the main active kind for degradation of MB; only small amounts of $^{\bullet}O_2^-$ free radical are formed and converted into $^{\bullet}OH$ free radical. The main degradation pathway of MB is eq 1. As shown Figure 10b, the degradation rate of MO dropped to 32.16% with addition of DMSO, which showed that $^{\bullet}OH$ radicals are the major active kind for MO. The degradation rate of MO decreased sharply to 17.21% with addition of BQ. The fact indicates that the main source of $^{\bullet}OH$ radicals is $^{\bullet}O_2^-$, which has further proved that photogenerated hole for MO is meaningless. The main degradation pathway of MO is eqs 1 → eq 2 → eq 3 → eq 4. The degradation rate of RHB reduced to 12.26% and 74.85% with addition of BQ and DMSO, respectively (Figure 10c). The level of decline for the former is much smaller than that for the latter, which indicates only a small number of $^{\bullet}OH$ radicals are generated by $^{\bullet}O_2^-$ radicals. Thus, $^{\bullet}O_2^-$ radicals are more important to active material than $^{\bullet}OH$ radicals. The fact implies that photogenerated holes are negligible for degradation of RHB. The

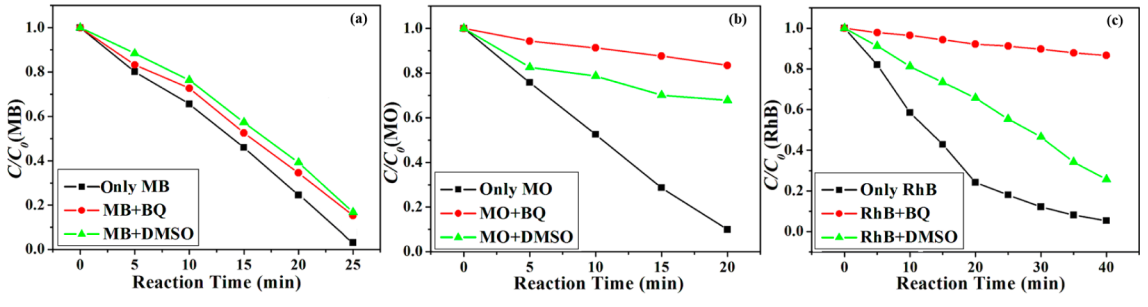

Figure 10. Dynamic curves of MB (a), MO (b), and RhB (c) degradation over compound **1** with added radical scavengers under UV-light.

DOI: 10.1021/acs.inorgchem.5b00508
Inorg. Chem. 2015, 54, 6744−6757

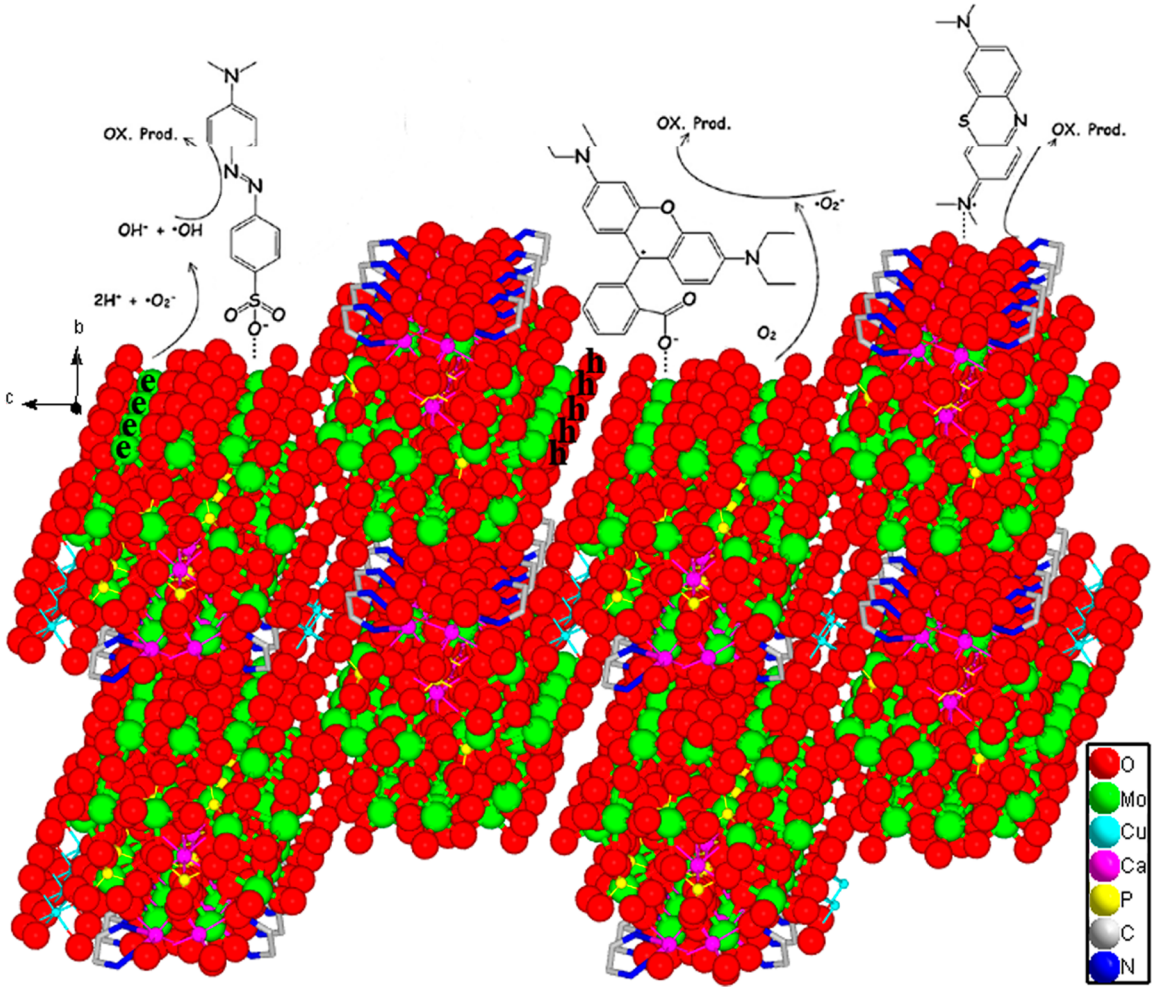

Figure 11. Degradation schematic of MB, MO, and RhB on the surface of compound **1**.

possible photoreaction pathways for MB, MO, and RHB on the surface of compound **1** are shown in Figure 11.

Basket-like catalysts are more efficient and quicker than other reported POM materials. In our system, basket-like heteropoly blue may better synergistically catalyze than other POM ions or the special structure of basket-like POM makes electrons and holes migrate to the surface of the basket cage rapidly, thus the photocatalytic activities improved significantly.

Electrochemical and Electrocatalytic Properties. *Cyclic Voltammetric Behaviors of 1−4-Carbon Paste Electrodes (CPE).* The electrochemical behaviors of compounds **1**−**4** were explored in 1 mol/L H_2SO_4 aqueous solution at diverse sweep speeds. As shown in Figures S16 and S17, Supporting Information, three pairs of reversible redox peaks are detected for **1**−**4**-CPE from 1.0 to −1.0 V. The average peak potentials $E_{1/2} = 1/2(E_{pa} + E_{pc})$ of I/I′ and III/III′ are −0.299 and 0.499 V for **1**-CPE, −0.319 and 0.526 V for **2**-CPE, −0.301 and 0.521 V for **3**-CPE, −0.302 and 0.506 V for **4**-CPE, which are ascribed to the redox processes of Mo in the basket-like framework. In addition, the redox peaks II−II′ at $E_{1/2}$ = 0.076 V for **1**, 0.078 V for **2**, 0.062 V for **3**, and 0.065 V for **4** are attributed to the Cu^{II} or Fe^{II} redox process.[14,15] The differences in the peak positions among compounds **1**−**4** are attributed to the incorporation of different metal ions or the different coordination environments around metal in their covalent framework, which cause their different redox characteristics. The plots of the peak currents (II) of anode and cathode against scanning rates are shown in Figure S16, Supporting Information. The peak currents were proportional to the sweep speed at the sweep speed less than 100 mV s^{-1}, while at scan speed more than 100 mV s^{-1}, the peak currents were proportional to the square root of the scanning speed, showing surface-controlled redox processes at scanning rates lower than 100 mV s^{-1} and diffusion-controlled redox processes at scanning rates higher than 100 mV s^{-1}.[29]

Bifunctional Electrocatalytic Activities of 1−4-CPE. The electrocatalytic properties of **1**−**4**-CPEs have also been investigated. As shown in Figure 12, with the potential from +1.0 to −1.0 V, with the increase of the concentration for NO_2^-, all the reduction peak currents of **1**−**4**-CPE increase while the corresponding oxidation peak currents decrease, showing that NO_2^- was reduced by the four species of basket-like polyoxoanion. In addition, **1**−**4**-CPEs also exhibit catalytic oxidation abilities toward amino acids (AAs). As shown in Figure 13, the oxidation and reduction peak currents of the third pairs of wave III−III′ both increase accompanying the increase of the concentration of AAs; however, the extent of increase for oxidation peak currents are much higher than the reduction peak currents. In contrast, the electroreduction of H_2O_2 and oxidation of AAs at a naked electrode usually needs a high overpotential, and no obvious response was detected at a bare CPE. All these results indicate that **1**−**4**-CPEs have

DOI: 10.1021/acs.inorgchem.5b00508
Inorg. Chem. 2015, 54, 6744−6757

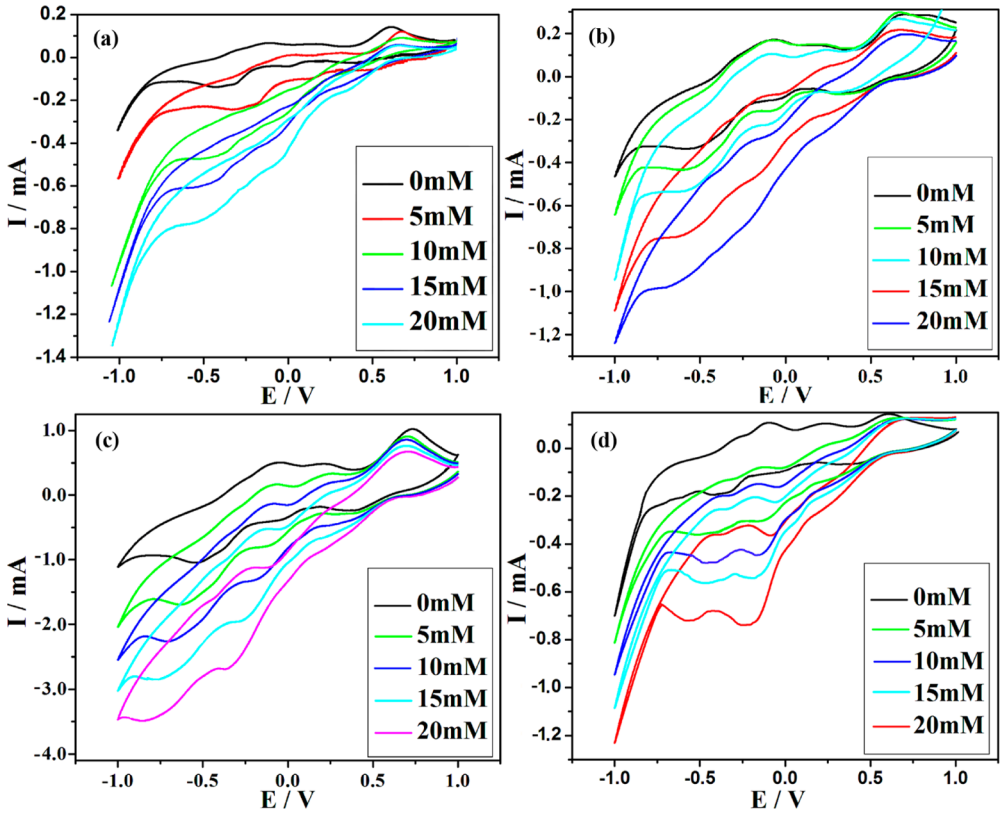

Figure 12. Cyclic voltammograms of (a) **1**-, (b) **2**-, (c) **3**-, and (d) **4**-CPE in 1 M H_2SO_4 solution containing nitrite at different concentrations (Potentials vs SCE. Scan rate 60 $mV{\cdot}s^{-1}$).

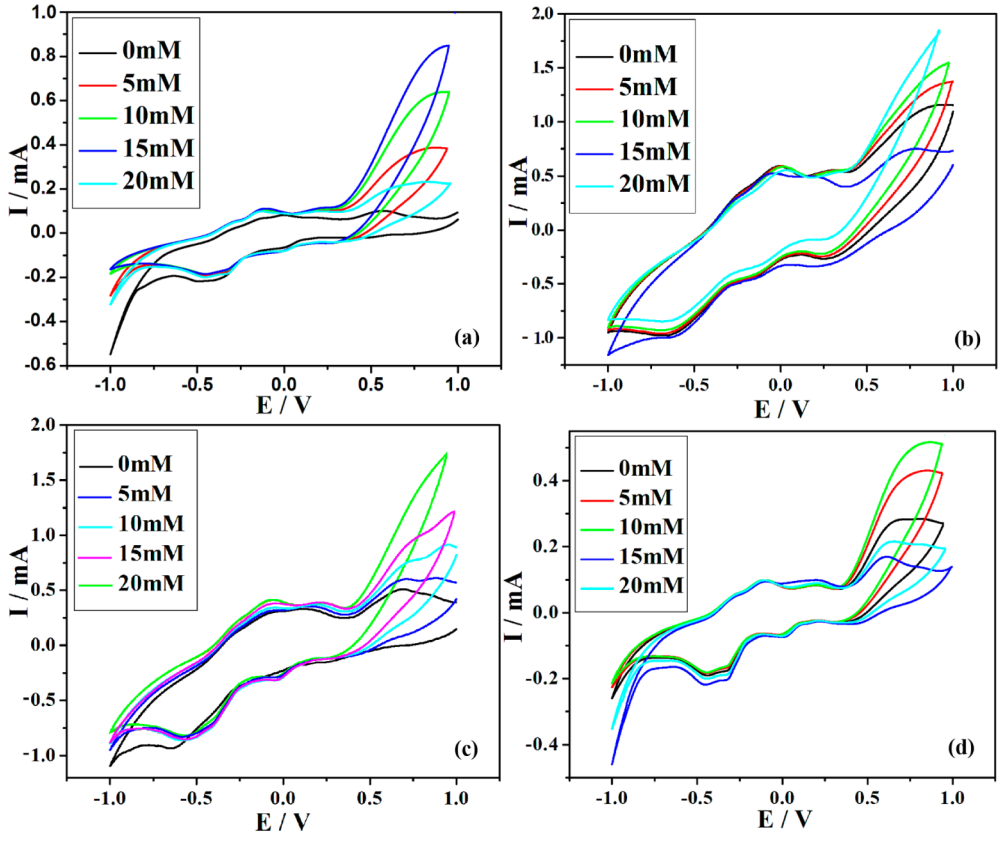

Figure 13. Cyclic voltammograms of (a) **1**-, (b) **2**-, (c) **3**-, and (d) **4**-CPE in 1 M H_2SO_4 solution containing AAs at different concentrations (Potentials vs SCE. Scan rate 60 $mV{\cdot}s^{-1}$).

DOI: 10.1021/acs.inorgchem.5b00508
Inorg. Chem. 2015, 54, 6744−6757

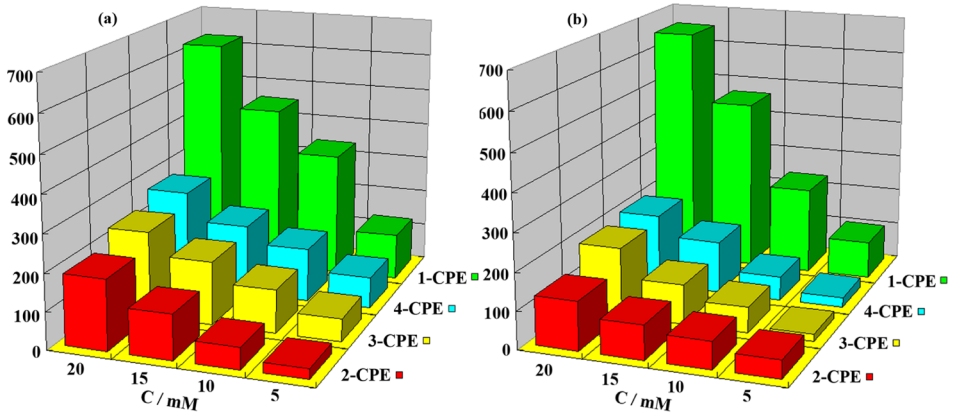

Figure 14. CAT vs concentration of (a) NO_2^- and (b) AAs for **1**−**4**-CPE. (I_p values of cathodic peak I for NO_2^- and anodic peak III for AAs at a scan rate of 60 $mV \cdot s^{-1}$).

bifunctional electrocatalytic activities toward not only reduction of normal inorganic molecules NO_2^- but also oxidation of biological molecules, AAs.

The electrocatalytic efficiency (CAT) of **1**−**4**-CPEs can be defined as

$$\mathrm{CAT} = 100\% \times [I_p(\mathrm{POM, substrate}) - I_p(\mathrm{POM})] / I_p(\mathrm{POM})]$$

where I_p(POM, substrate) and I_p(POM) are the peak currents for the reduction of the POM with and without the presence of substrate (NO_2^-, AAs), respectively.[30] As shown in Figure 14, **1**-CPE shows a higher CAT value toward both reduction of NO_2^- and oxidation of AAs, which indicates that the introduction of tetranuclear calcium complexes may be conductive to the electron transfer during the electrocatalytic process. The **3**- and **4**-CPE show the similar CAT values toward electrocatalysis of both NO_2^- and AAs. The similar 1-D chain structrures for compounds **3** and **4** are the main reason for the results. In addition, **2**-CPE shows a lower CAT value than the other CPEs, which may be due to the severe steric effects and less bth ligand impeding electron exchange in the highly connected basket layer structure.

CONCLUSIONS

The dimensions of basket-like POMs are successfully extended to two-dimensional layers by introduction of polynuclear complex bridges and activation of oxygen atoms in the "basket body" positions. The diffuse reflectivity spectrum shows that compounds **1**−**4** can be regarded as wide gap semiconductors, which exhibit universal highly efficient degradation ability for typical dyes such as MB, MO, and RhB under UV light. The catalysts have excellent repeatability and stability. The photocatalytic pathways are investigated by a series of radical trapping experiments. In addition, the compounds also indicate good bifunctional electrocatalytic behavior for oxidation of AAs and reduction of NO_2^-. This work enriches basket-like inorganic−organic hybrid materials and provides a useful prototype for design and synthesis of 3D highly connected basket-like hybrid compounds.

ASSOCIATED CONTENT

Supporting Information

Crystallographic data in CIF format, tables of selected bond lengths (Å) and bond angles (deg) for compounds **1**−**4**; IR, UV, TG, and CV behaviors of compounds **1**−**4**, ORTEP plots and partial structural figures of compounds **1**−**4**. The Supporting Information is available free of charge on the ACS Publications website at DOI: 10.1021/acs.inorgchem.5b00508.

AUTHOR INFORMATION

Corresponding Authors

*E-mail: hlyukai188@163.com (K. Yu).
*E-mail: zhou_bai_bin@163.com (B.B. Zhou).

Notes

The authors declare no competing financial interest.

ACKNOWLEDGMENTS

This work was supported the National Natural Science Foundation of China (Grants Nos. 21371042 and 21271056), the Ministry of Education and Specialised Research Fund for the Doctoral Program of Higher Education (Grant 20122329110001), the Natural Science Foundation of Heilongjiang Province (ZD2015001), Key Laboratory of Functional Inorganic Material Chemistry (Heilongjiang University), Ministry of Education, Doctoral initiation Foundation of Harbin Normal University (No. KGB201213), and Program for Scientific and Technological Innovation Team Construction in Universities of Heilongjiang Province (No. 2011TD010).

REFERENCES

(1) (a) Gouzerh, P.; Proust, A. *Chem. Rev.* **1998**, *98*, 77. (b) Hueber, D.; Hoffmann, M.; Louis, B.; Pale, P.; Blanc, A. *Chem. - Eur. J.* **2014**, *20*, 3903.

(2) (a) Getman, R. B.; Bae, Y. S.; Wilmer, C. E.; Snurr, R. Q. *Chem. Rev.* **2012**, *112*, 703. (b) Suh, M. P.; Park, H. J.; Prasad, T. K.; Lim, D. W. *Chem. Rev.* **2012**, *112*, 782. (c) Li, J. R.; Tao, Y.; Yu, Q.; Bu, X. H.; Sakamoto, H.; Kitagawa, S. *Chem. - Eur. J.* **2008**, *14*, 2771. (d) Liu, D.; Lu, Y.; Tan, H. Q.; Chen, W. L.; Zhang, Z. M.; Li, Y. G.; Wang, E. B. *Chem. Commun.* **2013**, *49*, 3673.

(3) (a) Long, D. L.; Burkholder, E.; Cronin, L. *Chem. Soc. Rev.* **2007**, *36*, 105. (b) Lydon, C.; Busche, C.; Miras, H. N.; Delf, A.; Long, D. L.; Yellowlees, L.; Cronin, L. *Angew. Chem., Int. Ed.* **2012**, *51*, 2115. (c) Zeng, Y. F.; Hu, X.; Liu, F. C.; Bu, X. H. *Chem. Soc. Rev.* **2009**, *38*, 469. (d) Wang, X. Q.; Liu, S. X.; Liu, Y. W.; He, D. F.; Li, N.; Miao, J.; Ji, Y. J.; Yang, G. Y. *Inorg. Chem.* **2014**, *53*, 13130.

(4) (a) Horcajada, P.; Gref, R.; Baati, T.; Allan, P. K.; Maurin, G.; Couvreur, P.; Férey, G.; Morris, R. E.; Serre, C. *Chem. Rev.* **2012**, *112*, 1232. (b) Stroobants, K.; Moelants, E.; Giang T. Ly, H.; Proost, P.; Bartik, K.; Parac-Vogt, T. N. *Chem. - Eur. J.* **2013**, *19*, 2848.

DOI: 10.1021/acs.inorgchem.5b00508
Inorg. Chem. 2015, 54, 6744−6757

(5) (a) Papaconstantinou, E. *Chem. Soc. Rev.* **1989**, *18*, 1. (b) Du, M.; Guo, Y. M.; Chen, S. T.; Bu, X. H.; Batten, S. R.; Ribas, J.; Kitagawa, S. *Inorg. Chem.* **2004**, *43*, 1287. (c) Zhao, C. C.; Glass, E. N.; Chica, B.; Musaev, D. G.; Sumliner, J. M.; Dyer, R. B.; Lian, T. Q.; Hill, C. L. *J. Am. Chem. Soc.* **2014**, *136*, 12085. (d) Omwoma, S.; Gore, C. T.; Ji, Y. C.; Hu, C. W.; Song, Y. F. *Coord. Chem. Rev.* **2015**, *286*, 17.

(6) (a) Xiao, F. p.; Hao, J.; Zhang, J.; Lv, C. L.; Yin, P. C.; Wang, L. S.; Wei, Y. G. *J. Am. Chem. Soc.* **2010**, *132*, 5956. (b) Lv, H. J.; Guo, W. W.; Wu, K. F.; Chen, Z. Y.; Bacsa, J.; Musaev, D. G.; Geletii, Y. V.; Lauinger, S. M.; Lian, T. Q.; Hill, C. L. *J. Am. Chem. Soc.* **2014**, *136*, 14015. (c) Lü, J.; Lin, J. X.; Zhao, X. L.; Cao, R. *Chem. Commun.* **2012**, *48*, 669.

(7) (a) An, H. Y.; Hu, Y.; Wang, L.; Zhou, E. L.; Fei, F.; Su, Z. M. *Cryst. Growth Des.* **2015**, *15*, 164. (b) Liu, D.; Lu, Y.; Tan, H. Q.; Wang, T. T.; Wang, E. B. *Cryst. Growth Des.* **2015**, *15*, 103. (c) Chen, W. C.; Wang, X. L.; Jiao, Y. Q.; Huang, P.; Zhou, E. L.; Su, Z. M.; Shao, K. Z. *Inorg. Chem.* **2014**, *53*, 9486.

(8) (a) Huang, L.; Wang, S. S.; Zhao, J. W.; Cheng, L.; Yang, G. Y. *J. Am. Chem. Soc.* **2014**, *136*, 7637. (b) Zhou, J.; Zhao, J. W.; Wei, Q.; Zhang, J.; Yang, G. Y. *J. Am. Chem. Soc.* **2014**, *136*, 5065.

(9) (a) He, W. W.; Li, S. L.; Zang, H. Y.; Yang, G. S.; Zhang, S. R.; Su, Z. M.; Lan, Y. Q. *Coord. Chem. Rev.* **2014**, *279*, 141. (b) Liu, Y. W.; Yang, X.; Miao, J.; Tang, Q.; Liu, S. M.; Shi, Z.; Liu, S. X. *Chem. Commun.* **2014**, *50*, 10023.

(10) (a) Omwoma, S.; Gore, C. T.; Ji, Y. C.; Hu, C. W.; Song, Y. F. *Coord. Chem. Rev.* **2015**, *286*, 17−29. (b) Santoni, M. P.; Hanana, G. S.; Hasenknopf, B. *Coord. Chem. Rev.* **2014**, *281*, 64. (c) Li, S. B.; Ma, H. Y.; Pang, H. J.; Zhang, L. *Cryst. Growth Des.* **2014**, *14*, 4450.

(11) (a) Liang, M. X.; Ruan, C. Z.; Sun, D.; Kong, X. J.; Ren, Y. P.; Long, L. S.; Huang, R. B.; Zheng, L. S. *Inorg. Chem.* **2014**, *53*, 897. (b) Dong, H.; Yang, Y. N.; Zhao, F. F.; Zhang, G. J.; Hu, H. L.; Kang, Z. H. *CrystEngComm* **2014**, *16*, 3624. (c) Sha, J. Q.; Sun, J. W.; Wang, C.; Li, G. M.; Yan, P. F.; Li, M. T. *Cryst. Growth Des.* **2012**, *12*, 2242. (d) Wang, L.; Yang, W. T.; Zhu, W.; Guan, X. G.; Xie, Z. G.; Sun, Z. M. *Inorg. Chem.* **2014**, *53*, 11584. (e) Zhang, C.; Lin, X.; Zhang, Z.; Long, L. S.; Wang, C.; Lin, W. *Chem. Commun.* **2014**, *50*, 11591.

(12) (a) Meyer, L. A.; Haushalter, R. C. *Inorg. Chem.* **1993**, *32*, 1579. (b) Mundi, L. A.; Haushalter, R. C. *Inorg. Chem.* **1992**, *31*, 3050. (c) Chang, W. J.; Jing, Y. C.; Wang, S. L.; Lii, K. H. *Inorg. Chem.* **2006**, *45*, 6586. (d) Zhang, W. S.; Gong, J. J.; Zhang, L. L.; Yang, Y. N.; Liu, Y.; Zhang, H. C.; Zhang, G. J.; Dong, H.; Hu, H. L.; Zhao, F. F.; Kang, Z. H. *Dalton Trans.* **2013**, *42*, 1760. (e) Du, D. Y.; Qin, J. S.; Wang, T. T.; Li, S. L.; Su, Z. M.; Shao, K. Z.; Lan, Y. Q.; Wang, X. L.; Wang, E. B. *Chem. Sci.* **2012**, *3*, 705.

(13) (a) Finn, R. C.; Rarig, R. S.; Zubieta, J. *Inorg. Chem.* **2002**, *41*, 2109. (b) Jin, H. J.; Zhou, B. B.; Yu, Y.; Zhao, Z. F.; Su, Z. H. *CrystEngComm* **2011**, *13*, 585. (c) Thomas, J.; Ramanan, A. *Cryst. Growth Des.* **2008**, *8*, 3390. (d) Shestakova, P.; Absillis, G.; Martin-Martinez, F. J.; Proft, F. D.; Willem, R.; Parac-Vogt, T. N. *Chem. - Eur. J.* **2014**, *20*, 5258. (e) Li, Z. L.; Wang, Y.; Zhang, L. C.; Wang, J. P.; You, W. S.; Zhu, Z. M. *Dalton Trans.* **2014**, *43*, 5840. (f) Wang, Y.; Pan, S. L.; Yu, H. W.; Su, X.; Zhang, M.; Zhang, F. F.; Han, J. *Chem. Commun.* **2013**, *49*, 306. (g) Li, X. M.; Chen, Y. G.; Su, C. N.; Zhou, S.; Tang, Q.; Shi, T. *Inorg. Chem.* **2013**, *52*, 11422. (h) Dey, C.; Kundu, T.; Banerjee, R. *Chem. Commun.* **2012**, *48*, 266.

(14) Zhang, X. M.; Wu, H. S.; Zhang, F. Q.; Prikhod'ko, A.; Kuwata, S.; Comba, P. *Chem. Commun.* **2004**, 2046.

(15) Yu, K.; Li, Y. G.; Zhou, B. B.; Su, Z. H.; Zhao, Z. F.; Zhang, Y. N. *Eur. J. Inorg. Chem.* **2007**, *2007*, 5662.

(16) Zhang, F. Q.; Zhang, X. M.; Fang, R. Q.; Wu, H. S. *Dalton Trans.* **2010**, *39*, 8256.

(17) Yu, K.; Wan, B.; Yu, Y.; Wang, L.; Su, Z. H.; Wang, C. M.; Wang, C. X.; Zhou, B. B. *Inorg. Chem.* **2013**, *52*, 485.

(18) Yu, K.; Zhou, B. B.; Yu, Y.; Su, Z. H.; Wang, H. Y.; Wang, C. M.; Wang, C. X. *Dalton Trans.* **2012**, *41*, 10014.

(19) (a) Yu, K.; Zhou, B. B.; Yu, Y.; Su, Z. H.; Yang, G. Y. *Inorg. Chem.* **2011**, *50*, 1862. (b) Wang, Y.; Xu, L.; Jiang, N.; Zhao, L. L.; Li, F. Y.; Liu, X. Z. *CrystEngComm* **2011**, *13*, 410. (c) Shen, Y.; Peng, J.; Zhang, H. Q.; Chen, C. Y.; Zhang, F.; Bond, A. M. *J. Mater. Chem.* **2011**, *21*, 6995.

(20) (a) Streb, C.; Long, D. L.; Cronin, L. *Chem. Commun.* **2007**, 471. (b) Streb, C.; Long, D. L.; Cronin, L. *CrystEngComm* **2006**, *8*, 629. (c) She, S.; Bian, S. T.; Hao, J.; Zhang, J. W.; Zhang, J.; Wei, Y. G. *Chem. - Eur. J.* **2014**, *20*, 16987.

(21) (a) Barrows, J. N.; Jameson, G. B.; Pope, M. T. *J. Am. Chem. Soc.* **1985**, *107*, 1771. (b) Dablemont, C.; Proust, A.; Thouvenot, R.; Afonso, C.; Fournier, F.; Tabet, J. C. *DaltonTrans.* **2005**, 1831. (c) Zhang, X.; Yi, Z. H.; Zhao, L. Y.; Chen, Q.; Gu, X. M.; Xu, J. Q.; Wang, X. L.; Yang, C.; Xu, X. Z.; Xia, W. J. *Dalton Trans.* **2009**, 9198. (d) Liu, B.; Yang, J.; Yang, G. C.; Ma, J. F. *Inorg. Chem.* **2013**, *52*, 84. (e) Hao, X. L.; Ma, Y. Y.; Wang, Y. H.; Zhou, W. Z.; Li, Y. G. *Inorg. Chem. Commun.* **2014**, *41*, 19.

(22) (a) Sheldrick, G. M. *SHELXL 97, Program for Crystal Structure Refinement*; University of Göttingen, Germany, 1997. (b) Sheldrick, G. M. *SHELXL 97, Program for Crystal Structure Solution*; University of Göttingen, Germany, 1997.

(23) (a) Brown, I. D.; Altermatt, D. *Acta Crystallogr., Sect. B: Struct. Sci.* **1985**, *41*, 244. (b) Liu, W.; Thorp, H. H. *Inorg. Chem.* **1993**, *32*, 4102.

(24) Pope, M. T. *Heteropoly and Isopoly Oxometalates*; Springer-Verlag: Berlin, 1983.

(25) Patterson, T. A.; Carver, J. C. D.; Leyden, E.; Hercules, D. M. *J. Phys. Chem.* **1976**, *80*, 1700.

(26) (a) Pankove, J. I. *Optical Processes in Semiconductors*; Prentice Hall: Englewood Cliffs, NJ, 1971. (b) Wesley, W. M.; Harry, W. G. H. *Reflectance Spectroscopy*; Wiley: New York, 1966.

(27) (a) Wang, X. L.; Li, N.; Tian, A. X.; Ying, J.; Li, T. J.; Lin, X. L.; Luan, J.; Yang, Y. *Inorg. Chem.* **2014**, *53*, 7118. (b) Lin, H.; Maggard, P. A. *Inorg. Chem.* **2008**, *47*, 8044. (c) Hu, Y.; Luo, F.; Dong, F. F. *Chem. Commun.* **2011**, *47*, 761. (d) Wu, Q.; Chen, W. L.; Liu, D.; Liang, C.; Li, Y. G.; Lin, S. W.; Wang, E. B. *Dalton Trans.* **2011**, *40*, 56.

(28) Marcì, G.; García-López, E. I.; Palmisano, L. *Eur. J. Inorg. Chem.* **2014**, *2014*, 21.

(29) Dong, S.; Xi, X.; Tian, M. *J. Electroanal. Chem.* **1995**, *385*, 227.

(30) Keita, B.; Belhouari, A.; Nadjo, L.; Contant, R. *J. Electroanal. Chem.* **1995**, *381*, 243.

DOI: 10.1021/acs.inorgchem.5b00508
Inorg. Chem. 2015, 54, 6744−6757